Articles

Effect of Methanol Concentration on CTAB Micellization and on the Formation of Surfactant-Templated Silica (STS)

Mark T. Anderson,*,† James E. Martin, Judy G. Odinek, and Paula P. Newcomer

Encapsulants and Porous Materials Department and Nanostructures and Advanced Materials Chemistry Department, Sandia National Laboratories, Albuquerque, New Mexico 87185

Received April 17, 1997. Revised Manuscript Received March 25, 1998

We use light-scattering techniques to study the effects of methanol concentration on alkaline, cetyltrimethylammonium bromide (CTAB) water:methanol micellar solutions. We use X-ray diffraction, SEM, TEM, ^{29}Si NMR, and gas sorption measurements to study the structure, microstructure, and porosity of surfactant-templated silica (STS), synthesized by adding tetramethoxysilane (TMOS) to the above micellar solutions. The measured critical micelle concentration (cmc) for CTAB at 25 °C in a 0.22 M NaOH (pH 13.2) solvent increases from $\sim 1.3 \times 10^{-3}$ M for $r = 0\%$ to $\sim 5.5 \times 10^{-2}$ M for $r = 60\%$ (where r is the wt % methanol in the mixture) as the concentration of methanol increases. In turn, the long-range order of STS decreases as the methanol concentration increases. Ordered STS forms for $0 \leq r < 60\%$, where the concentration of CTAB, c, is greater than cmc in the precursor solution; disordered STS (resembling wormlike micelles) forms for $60 \leq r \leq 90\%$, where $c <$ cmc. For $r > 90\%$ transparent, amorphous chemical gels form. The presence of methanol leads to a uniform submicron microstructure as compared to faceted 1−10-μm particles with pure water. After template removal, apparent BET surface areas for STS can exceed 950 m^2/g, and the void volume can exceed 0.6 cm^3/g. Initially, there is a high fraction of uncondensed silica in the as-made product ($Q^3/Q^4 \approx 2.1$), but after calcination a strong, bonded siloxane framework forms ($Q^3/Q^4 \approx 0.40$).

1. Introduction

Surfactant-templated silica (STS) can be synthesized by assembling an inorganic phase around organic surfactants.[1−6] These templated materials are unique in that they have unimodal, narrow pore size distributions and their pore sizes are tunable from ∼15 to ∼100 Å. A wide variety of uses for STS have been demonstrated or contemplated, including use as acid catalysts[7−9] (although acidity is less than for zeolites),[6,10] oxidative catalysts for bulky organics,[11−13] supports for noble-metal oxidation and hydrogenation catalysts,[13] supports for NiMo in hydrocracking applications,[14] supports for heteropolyacid ion catalysts,[15,16] hosts for conducting polyaniline filaments[17] and carbon wires,[18] separations media (especially in membrane form), coatings for sensors,[19] and high surface area adsorbents.[1]

To synthesize STS, four reagents are required: a silica source, water, a catalyst, and a surfactant.[1−6] In a typical synthesis, a silica source is added to an

† New permanent address: Ceramic Technology Center, Industrial and Consumer Sector Research Laboratory, 3M Center, Bldg. 201-4N-01, St. Paul, MN 55144-1000.

(1) Beck, J. S.; Vartuli, J. C.; Roth, W. J.; Leonowicz, M. E.; Kresge, C. T.; Schmitt, K. D.; Chu, C. T.-W.; Olson, K. H.; Sheppard, E. W.; McCullen, S. B.; Higgins, J. B.; Schlenker, J. L. *J. Am. Chem. Soc.* **1992**, *114*, 10834−10843.
(2) Kresge, C. T.; Leonowicz, M. E.; Roth, W. J.; Vartuli, J. C.; Beck, J. S. *Nature* **1992**, *359*, 710−712.
(3) Huo, Q.; Margolese, D. I.; Ciesla, U.; Feng, P.; Gier, T. E.; Sieger, P.; Leon, R.; Petroff, P. M.; Schuth, F.; Stucky, G. D. *Nature* **1994**, *24*, 317−321.
(4) Huo, Q.; Margolese, D. I.; Ciesla, U.; Demuth, D. G.; Feng, P.; Gier, T. E.; Sieger, P.; Firouzi, A.; Chmelka, B. F.; Schuth, F.; Stucky, G. D. *Chem. Mater.* **1994**, *6*, 1176−1191.
(5) Tanev, P. T.; Pinnavaia, T. J. *Science* **1995**, *267*, 865−867.
(6) Chen, C.-Y.; Li, H.-X.; Davis, M. E. *Microporous Mater.* **1993**, *2*, 17−26.
(7) Kloetstra, K. R.; van Bekkum, H. J. *Chem. Res. Synop.* **1995**, *1*, 26−27.
(8) Armengol, E.; Maria, L.; Corma, A.; Garcia, G.; Navarro, M. T. *J. Chem. Soc., Chem. Commun.* **1995**, *5*, 519−520.
(9) Kloetstra, K. R.; van Bekkum, H. *J. Chem. Soc., Chem. Commun.* **1995**, *10*, 1005−1006.
(10) Corma, A.; Fornes, V.; Navarro, M. T.; Perez-Pariente, J. *J. Catal.* **1994**, *148*, 569.
(11) Corma, A.; Navarro, M. T.; Perez-Pariente, J. *J. Chem. Soc., Chem. Commun.* **1994**, 147.
(12) Tanev, P. T.; Chibwe, M.; Pinnavaia, T. J. *Nature* **1994**, *368*, 321.
(13) Schuth, F. *Ber. Bunsen-Ges.* **1995**, *99* (11), 1306−1315.
(14) Corma, A.; Martinez, A.; Martinez-Soria, V.; Monton, J. B. *J. Catal.* **1995**, *153*, 25.
(15) Kresge, C. T.; Marler, D. O.; Rav, G. S.; Rose, B. H. U.S. Patent 5,366,945, 1994.
(16) Kozhevnikov, I. V.; Sinnema, A.; Jansen, R. J. J., Pamin, K.; van Bekkum, H. *J. Catal. Lett.* **1995**, *30*, 241−252.
(17) Wu, C.-G.; Bien, T. *Science* **1994**, *264*, 1757−1759.
(18) Wu, C.-G.; Bien, T. *Science* **1994**, *266*, 1013.
(19) Olson, D. H.; Stucky, G. D.; Vartuli, J. C. U.S. Patent 5,364,797, 1994.

S0897-4756(97)00240-8 CCC: $15.00
Published on Web 04/30/1998

Table 1. Molar Ratios and Data for Water:Methanol Syntheses

r (%)	H_2O	methanol	TMOS	CTAB	NaOH	CSD (nm)[a]	yield (%)[b]	t_{gel} (s)[c]	*a* (Å)[d]
0	129.6	0.0	1	0.130	0.289	74	87.3	5.5 (1)	42.95 (14)
10	116.7	7.3	1	0.130	0.289	68	91.9	5 (1)	42.01 (8)
20	103.8	14.5	1	0.130	0.289	95	92.9	5 (1)	41.21 (5)
25	97.4	18.1	1	0.130	0.289	140[e]		5 (1)	*f*
30	90.9	21.8	1	0.130	0.289	58	97.5	5 (1)	40.60 (23)
40	78.0	29.0	1	0.130	0.289	50	98.5	5.5 (1)	39.69 (13)
50	65.1	36.3	1	0.130	0.289	40	97.3	6 (1)	38.61 (26)
60	52.2	43.5	1	0.130	0.289	47	94.4	6.5 (1)	40.8 (3)
70	39.3	50.8	1	0.130	0.289	10	92.9	9 (1)	N/A
80	26.4	58.2	1	0.130	0.289	N/A[g]	83	12 (1)	N/A
90	13.5	65.3	1	0.130	0.289	N/A	91.7	36 (2)	N/A
100	0.6	72.6	1	0.130	0.289	N/A		>540	N/A

[a] Coherent scattering domain size from Scherrer equation (see eq 2). [b] Yield of solid phases (yield = 100(1 − ((mass of filtrate residue - calculated mass of NaBr)/theoretical yield of $SiO_{2.13}$·0.13 CTA^+))). In these samples the calculated mass of NaBr is ∼0.07 g, assuming all of the bromide ions are extracted. [c] Time after TMOS is added for the solution to form an opaque physical gel (or a transparent chemical gel in the case of $r = 100\%$). [d] Cell constant for powders aged 1 day at room temperature in their pore fluid (XRD data from these samples used to determine CSD). [e] Prepared at 10 °C with C_{16}TMA HSO_4 as the surfactant. [f] See Table 2 for examples. [g] N/A, not able to determine from the data.

alkaline aqueous solution of a micelle-forming cationic surfactant.[1−4,6] The silica source is hydrolyzed and condensed to form multidentate, multicharged anions that can coordinate with the surfactant headgroups.[4] The silica species and the surfactants assemble into silica/surfactant arrays that form colloidal particles that generally precipitate.[1−6] Over an extended period of time, the silica condenses to form a bonded siloxane framework, with the evolution of much heat. The surfactant templates can then be removed by one of several processes to form the porous material.[1−6]

In the synthesis of STS several advantages are realized by the addition of a cosolvent to the reaction mixture; for methanol we find that (1) the silica source (TMOS)[20−24] is rapidly dissolved, which leads to homogeneous precursor solutions;[25] (2) nearly quantitative yields with respect to silica and surfactant can be achieved; (3) micellization of the surfactant is still possible in the precursor solution; in fact, the E hexagonal liquid crystalline phase forms in the simple CTAB/methanol system;[26] (4) the degree of order in the STS can be made greater than in a pure water system; (5) the micelle size, and consequently the cell constant and pore size of STS, can be tailored over several angstroms; and (6) it is possible to conveniently shift the micelle ↔ free surfactant equilibrium toward free surfactant, which allows the investigation of the ability of silicate ions to assist the organization of surfactant molecules into a liquid crystalline structure as the concentration of preformed surfactant templates is decreased.

In our previous work[20] we also noted an apparent correlation of STS long-range order with extent of surfactant micellization. Here, we use light scattering to characterize the extent of micellization in the water/methanol/surfactant/base solution as the methanol concentration is changed in 10 wt % increments. We examine the long-range order of the STS and show that both micellization and long-range order depend on methanol concentration, and further note that the most distinct changes in extent of micellization (cmc) occur at roughly the same methanol concentration as the change from an ordered to a disordered structure (from 3 to 1 Bragg peaks in XRD). The results presented here add to a small but growing literature on the synthesis of periodic mesoporous materials from water:cosolvent systems.[20,27]

2. Experimental Section

2.1 Synthesis. Table 1 shows the molar ratios of reagents used to synthesize STS. A typical synthesis involves mixing, in a 20-mL scintillation vial, 9.8 g of deionized water plus methanol (see Table 1 for molar ratios), and 0.2 g (0.55 mmol) of cetyltrimethylammonium bromide, $C_{19}H_{42}NBr$ (CTAB; Fisher, 99+%), to form a micellar solution. To this 2 wt % CTAB solution is added 65 μL of 50 wt % aqueous NaOH (1.14 mmol) and 0.625 mL (4.23 mmol) of tetramethoxysilane (TMOS, United Chemical Technologies or Aldrich). **WARNING: TMOS vapors can cause blindness; goggles should be worn.**

For water:methanol ratios greater than 10:90, w/w ($r < 90\%$, where $r \equiv$ weight percent methanol in the water/methanol/CTAB solution), the addition of TMOS causes the clear solution to turn opaque, as a white particulate gel forms. The resulting wet gels are aged in the pore fluid at ambient temperature for 1 min to 30 days (details given for each sample), suction

(20) (a) Anderson, M. T.; Martin, J. E.; Odinek, J.; Newcomer, P. *Chem. Mater.* **1998**, *10*, (1), 311−321. (b) The synthesis of STS with TMOS as the silica source leads to important and interesting differences compared to products made from other silica sources; these differences include: a significant effect on the tertiary structure of the product, giving gels rather than precipitates; a dramatic reduction in the time to make an ordered product (<10 s); pore diameters that can be continuously tailored over a ∼5-Å range; as-made silica/surfactant composites that have a high fraction of uncondensed silica species (after calcination, the extent of framework condensation is virtually identical to that for materials made hydrothermally or from TEOS); and materials in several useful forms, i.e., thin films,[21, 22] monolithic xerogels,[23] monolithic aerogels,[24] and powders of submicron particles (reported herein).

(21) Martin, J. E.; Anderson, M. T.; Odinek, J.; Newcomer, P. *Langmuir* **1997,** *13* (15), 4133−4141.

(22) Lu, Y.; Ganguli, R.; Drewien, C. A.; Anderson, M. T.; Brinker, C. J.; Gong, W.; Guo, Y.; Soyez, H.; Dunn, B.; Huang, M. H.; Zink, J. I. *Nature* **1997**, *389*, 364−368.

(23) Anderson, M. T.; Martin, J. E.; Odinek, J.; Newcomer, P. *Microporous Mater.* **1997,** *10* (1−3), 13−24.

(24) Anderson, M. T.; Sawyer, P. S.; Rieker, T. *Microporous Mesoporous Mater.*, in press.

(25) The four-reagent syntheses described above lead to formation of STS from inhomogeneous solutions, and thus can result in less than optimal yield (with respect to silica and surfactant, especially where nonmolecular silica sources are used along with a large molar excess of surfactant).

(26) Fontell, K.; Khan, A.; Lindström, B.; Maciejewska, D.; Puang-Ngern, S. *Colloid Polym. Sci.* **1991**, *269*, 727−742.

(27) (a) Kim, A. Y.; Liu, J.; Virden, J. W.; Bunker, B. *Materials Research Society Symposium Proceedings* Komarneni, S., Smith, D. M., Beck, J. S., Eds.; Materials Research Society: Pittsburgh, PA, 1995; Vol. 371, pp 105−110. (b) Vaudry, F.; Khodabandeh, S.; Davis, M. E. *Chem. Mater.* **1996**, *8* (7), 1451−1464.

filtered, washed with deionized water and/or methanol to remove excess surfactant and metal ions, and dried in air. The occluded surfactant typically is removed from the product by calcination in a tube furnace (details in Table 2).

2.2. X-ray Diffraction. Data were collected with a Scintag PAD V instrument using nickel-filtered Cu Kα radiation. Data were collected in continuous scan mode from 1.5 to 10° 2θ with a 0.02° sampling interval and a 1°/min scan rate. Slits widths starting from the source were 1, 2, 1, and 0.3 mm. Tube voltage was 45 kV, and tube current was 35 mA. Peak positions and full-widths at half-height were determined with Scintag analysis software (TC9 package). Peak positions for the periodic hexagonal phase were corrected with an external standard routine. The routine used four Bragg peaks (100, 110, 200, 210) for the correction.

2.3. Light Scattering. Dynamic and static light-scattering measurements were made with a 63-mW NEC He−Ne laser, using a 256-channel Langley-Ford correlator. A Malvern index-matching temperature-controlled scattering vat, a Malvern detector assembly using an RCA FW130 photomultiplier tube, and an Aerotech 12-in. stepper-motor-driven goniometer complete the basic light-scattering hardware. The system is automated by a DEC PDP-11/73b computer.

Intensity autocorrelation functions, $S_2(q,t) = \langle I(q,0)I(q,t)\rangle$, were collected, and the Seigert relation was used to obtain the field autocorrelation function, $S_1(q,t) = \langle E(q,0)E(q,t)\rangle$, from these.[28] The field autocorrelation function data were fit to single-exponential decays, and the micelle radius was determined from the heterodyne decay rate Γ from the standard relation $\Gamma = D_t q^2$, where q is the scattering wave vector and D_t is the translational diffusion constant. The Stokes−Einstein relation $D_t = k_B T/6\pi\eta R$ was then used to extract the radius.

The static intensity data were taken on the same instrument using a statistical procedure to discard anomalously high intensity readings due to dust. Filtration of all micelle samples in a clean bench reduced dust contamination.

2.4. ^{29}Si NMR. High-resolution, magic-angle spinning spectra were recorded on a Chemagnetics instrument equipped with a 4.7-T magnet. Powder samples were packed into 2.5 × 6 cm ZrO_2 rotors. Spectra were recorded at a resonance frequency of 39.7 MHz, with a 7.25-ms pulse at 90° and a pulse delay of 120 s. Final spectra are an average of 512 scans. Tetramethylsilane (TMS) was used as a standard to define 0 ppm. Data were analyzed and integrated with MacNMR software routines from Tecmag to determine Q ratios and shifts relative to TMS.

2.5. SEM/TEM. A JEOL 1200EX transmission electron microscope (TEM) with an ASID (SEM) attachment was used to observe the microstructure and grain size of the powder samples. To observe individual grains, the aggregated powders were ground under methanol with a mortar and pestle. The suspended powder was caught on the holey carbon film of a 3-mm copper grid. Bright-field TEM or diffraction contrast imaging was done at 120 kV and involved low (20 000×) and high (300 000×) magnifications of the individual grains and small aggregates. SEM micrographs were obtained that revealed the morphology of powder aggregates and the size of the grains.

Higher resolution images (up to 1 500 000×) were collected with a Phillips CM-30 TEM operated at an accelerating voltage of 300 keV. High values of defocus, generally negative, were used to show the mesoscale structure in the samples.

2.6. Gas Adsorption. A Micromeritics ASAP 2000 was used to collect isothermal N_2 adsorption data at 77 K. Samples were degassed overnight at 200 °C. Four-point BET analyses were performed to determine the apparent surface areas.

3. Results and Discussion

3.1. Homogeneous Solutions and Reaction Kinetics. Our initial goal was to form STS stoichiometrically from homogeneous solutions to avoid unwanted surfactant or silica byproducts. This requires a molecular silica source that is soluble in the solvent system. Many previous syntheses[1,2,6] have used colloidal or precipitated silica sources, such as fumed silica, precipitated silica, or water glass, but these are nonmolecular and are typically preformed with a large excess of surfactant. Other workers have used hydrophobic molecular sources, i.e., alkylsilanes. The syntheses are typically done in purely aqueous solutions.[3,4] Initially a water/alkoxysilane emulsion forms that can lead to unwanted siliceous byproducts.[29] For this reason we used a water:methanol solvent system that rapidly dissolves the molecular silica source TMOS.

As desired, TMOS in combination with methanol minimizes the time needed to dissolve the silica source.[30] Table 1 shows that the time it takes to form the wet gel (i.e. STS; see below) after TMOS is added to the precursor solution, t_{gel}, is on the order of only 5 s at room temperature. The products form so quickly that, for r < 25%, the alkoxide remains emulsified at the gel point (Figure 1) and the products form out of inhomogeneous solutions. For $r \geq 25\%$ the TMOS is solubilized prior to gel formation, and thus the amorphous silica byproducts (seed pods)[29] observed when when TMOS is mixed with pure water are eliminated (vide infra).

Figure 2 confirms that the wet gels that form in 5 s are STS at the earliest time we can make measurements, ∼1 min. The kinetics of STS formation with TMOS (i.e., <10 s) is 1−2 orders of magnitude faster than for TEOS[3,4] and 3−4 orders of magnitude faster for samples made from nonmolecular silica sources.[1,2,6] The hydrolysis time for alkoxysilanes increases as the size of the alkoxide ligand increases, which accounts for the difference between TEOS and TMOS. The relatively slow dissolution of solid colloidal silica probably accounts for the long times used to form mesophases derived from nonmolecular silica sources.

3.2. Methanol Suppresses Micelle Formation. As expected,[26,31,32] adding the lower dielectric constant cosolvent methanol to the water/CTAB/NaOH precursor solution changes the extent of micellization of the surfactant. To quantify the change, we applied static and dynamic light scattering in two ways. In the first method we simply took advantage of the fact that the scattering intensity above the solvent background $\Delta I(q)$ from a micelle solution[33] is

$$\Delta I(q) = bc'MS(q)f(qR) \qquad (1)$$

Here M is the micelle mass ($M = nm$, where n is the number of the surfactant molecules per micelle and m is the mass of a surfactant molecule), c' is the concentration of surfactant in the form of micelles, R is the radius of gyration of a micelle, $f(qR)$ is the micelle form

(28) Berne, B.; Pecora, R. *Dynamic Light Scattering*; Wiley: New York, 1976.

(29) We have directly observed with optical microscopy that the hydrolyzed TEOS forms micron-size seed-pod-like structures that eventually burst and expel partially hydrolyzed silicate species; the shell remains and is a contaminant in the final product.

(30) Cogan, J. D.; Setterstrom, C. A. *Chem. Eng. News* **1946**, *24*, 2499.

(31) Rosen, M. J. *Surfactants and Interfacial Phenomena*; Wiley: New York, 1989; Chapters 3 and 4.

(32) Myers, D. *Surfactant Science and Technology*; VCH: New York, 1992; Chapters 3 and 4.

(33) *Light Scattering in Liquids and Macromolecular Solutions*; DeGiorgio, V., Corti, M., Giglio, M., Eds.; Plenum: New York, 1980.

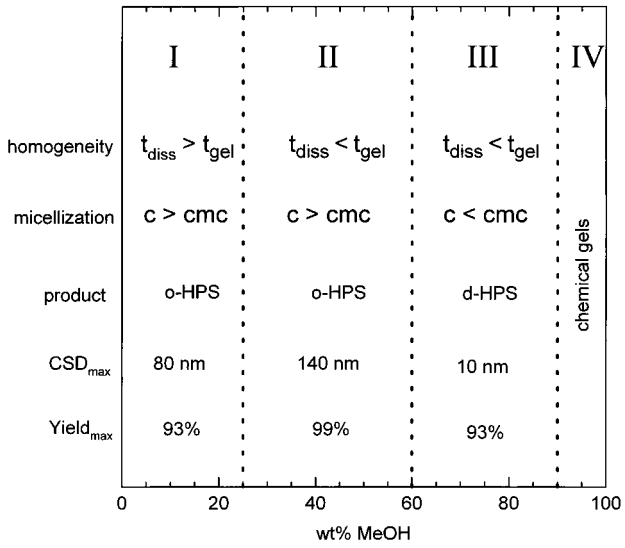

Figure 1. Four regions seen in the water:methanol system for samples made from the molar ratios shown in Table 1. The regions are defined by (1) precursor solution homogeneity (t_{diss} ≡ time required to solubilize TMOS as indicated by a translucent to transparent transformation; t_{gel} ≡ time to form a white physical gel); (2) extent of micellization [c is the wt % CTAB in the water:methanol solution (in all cases 2 wt %); cmc is the critical micelle concentration]; (3) type of product (o-HPS ≡ ordered surfactant-templated silica ≡ o-STS; d-HPS ≡ disordered surfactant-templated silica ≡ d-STS); (4) coherent scattering domain size, CSD; and (5) overall yield as defined in Table 1. In region I the solutions are inhomogeneous at the gel point ($t_{diss} > t_{gel}$); however, the concentration of micelles is highest in this region, so STS forms, but with less than optimal yield and less than optimal long-range order. In region II the solutions are homogeneous at the gel point; there are micelles, and STS forms with optimal long-range order and in highest yield. In region III the solutions are homogeneous; there are no micelles, and d-STS forms in less than optimal yield. In region IV solutions are homogeneous; there are no micelles, and only amorphous silica chemical gels form.

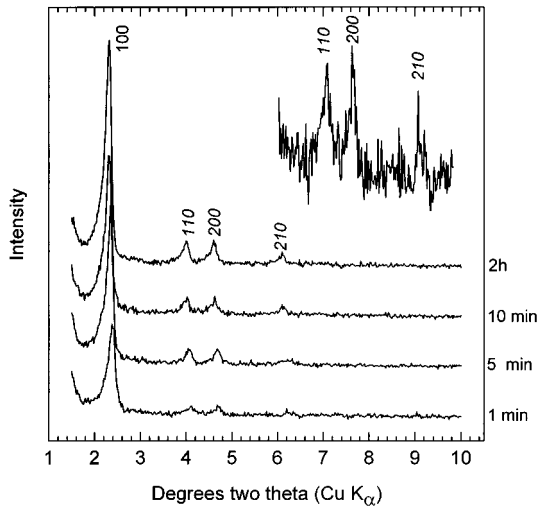

Figure 2. In situ X-ray diffraction of $r = 25\%$ wet gels aged for times shown on right. The wet gels were isolated by filtration and immediately transferred to an XRD holder. The inset shows the sample analyzed 1 min after the TMOS was added.

factor (conveniently expressed by a Bessel function) that gives the scattering from a single micelle, and $S(q)$ is the structure factor that gives the optical interference that arises from correlations between micelles, which

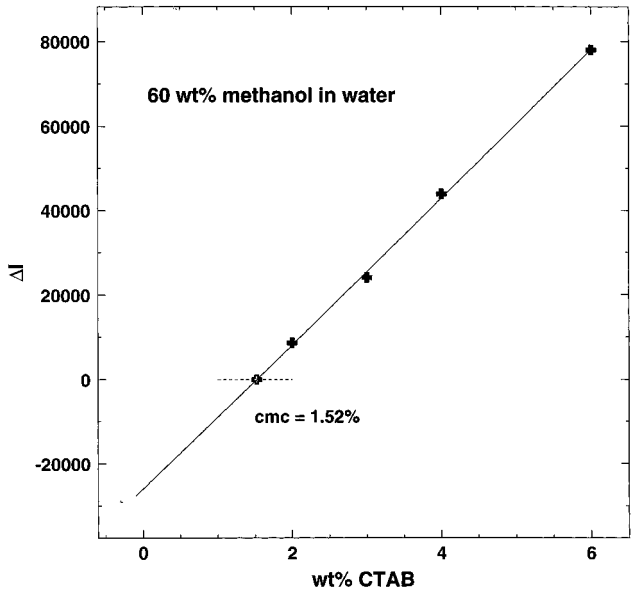

Figure 3. Static light scattering was used to determine the cmc by extrapolating the surfactant contribution to the light scattering to zero scattered intensity.

in turn are due to interactions between micelles. Finally, the q is scattering wave vector, $q = 4\pi \sin(\theta/2)/\lambda$, in terms of the scattering angle θ and the wavelength in the scattering medium, λ (633 nm/1.33), and b is a constant that depends on a variety of geometrical and optical factors, including the refractive index increment dn/dc. We assume here that the scattering from free surfactant is negligible.

The expression for the scattering intensity simplifies for small wave vectors and low concentration. When $qR \ll 1$, the intramicelle scattering interference is negligible and $f(qR \ll 1) \cong 1$. This condition is easily satisfied in our measurement, where $R \cong 2.5$ nm and $q \cong 1.05 \times 10^{-2}$ nm^{-1}. Likewise, when the concentration c of micelles is small, the intermicelle interference is negligible and $S(q) = 1$. Under these conditions $\Delta I(q) = bc'M$, and the concentration of micelles should simply be the concentration of surfactant, c, minus the concentration of free surfactant, which should be the critical micelle concentration, cmc, at least for concentrations close to the cmc, i.e., $DI(q) = b(c - \text{cmc})M$.

For $r = 0-70\%$ we thus studied the dependence of the micelle scattering intensity as a function of concentration and extrapolated these data to zero concentration (Figure 3) to find the cmc. From this study we found that the cmc increases significantly as the methanol concentration increases (Figure 4). The lower dielectric constant of methanol ($\epsilon = 33$ vs 78 for water) reduces the effectiveness of the chemical dipole of the surfactant, so that the exchange energy of placing a free surfactant into a micelle is less negative. The entropy of mixing of free surfactant is larger that the entropy of mixing of micelles, so the balance is shifted toward free surfactant.

The extrapolation in Figure 3 shows that the scattered intensity increases linearly with micelle concentration as long as the surfactant concentration is less that a few percent, implying that the intermicelle interference, which increases as the micelle concentration squared, is negligible. Thus, although at 2 wt %

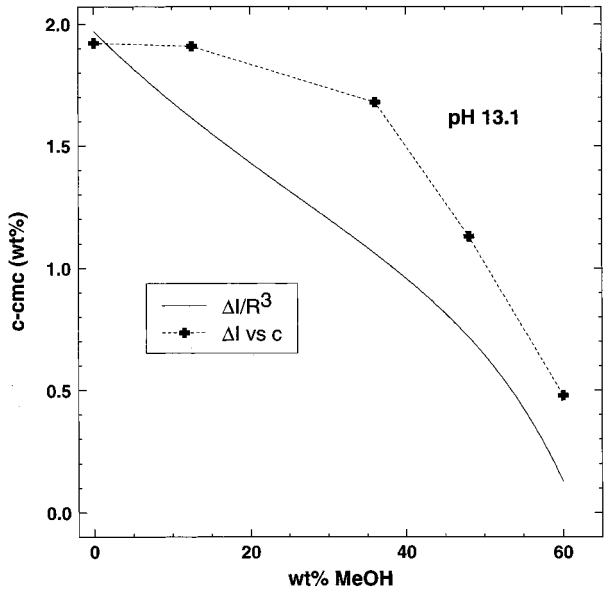

Figure 4. Amount of surfactant in the form of micelles in a water/methanol/CTAB/NaOH solution (molar ratios as in Table 1) determined by two methods: (1) determining the cmc as in Figure 3 and subtracting this from the surfactant concentration (2 wt %) and (2) dividing the measured scattering intensity of a 2 wt % CTAB solution by the cube of the hydrodynamic radius. The latter is the continuous line, obtained from the fits to the data in Figure 6. Although some discrepancies are observed in these two methods, the decrease in micellization with increasing methanol concentration is clear.

CTAB we are not in the strict limit of zero concentration, to a good approximation the relation $\Delta I(q) = b(c - \text{cmc})M$ holds.

The cmc can now be determined from the relation $c - \text{cmc} = \Delta I(q)/bM$. Of course, the micelle mass will in general depend on the solvent composition. We determined the micelle mass by measuring the hydrodynamic radius R_h of the micelle from the decay rate of the intensity autocorrelation function, using the Stokes–Einstein relation for the diffusion coefficient. The dependence of the micelle diffusion coefficient and the solvent viscosity on solvent composition is shown in Figure 5. The solvent composition dependence of the micelle hydrodynamic radius and solution scattering intensity is shown in Figure 6. The micelle mass was taken to be $M = aR_h^3$, so we finally have $c - \text{cmc} = \Delta I(q)/(baR_h^3)$. (Note that the refractive index of methanol, 1.326, is extremely close to that of water, 1.332, so that the variation in optical contrast is negligible.)

Concentration units can be obtained by noting that our measured cmc of CTAB in a pH 13.2 aqueous solution is 0.084% (i.e., 2.1×10^{-3} M, which is similar to the value of 9.2×10^{-4} M reported previously for CTAB in pure water).[34] Equating $\Delta I(q)/(baR_h^3)$ to $c - \text{cmc} = (2 - 0.076)$ gives us the product ab. We have plotted $c - \text{cmc}$ versus wt % MeOH in Figure 4, and these data are in reasonable agreement with the numbers computed by subtracting the measured cmc from the surfactant concentration.

Thus, despite the discrepancies between the two methods used to determine cmc, the general picture of the effect of methanol on micellization is clear: the concentration of surfactant in the form of micelles decreases rapidly as the methanol concentration increases (cmc $\approx 2.1 \times 10^{-3}$ M for $r = 0\%$, and cmc $\approx 5.5 \times 10^{-2}$ M for $r = 60\%$), until, at $r = 60\%$, the cmc is approximately equal to the surfactant concentration (i.e., 2%, or 5.5×10^{-2} M). For $r \geq 60\%$ all of the surfactant is in the form of free surfactant or aggregates too small to be detected with light scattering. In this case, it is reasonable to question whether the surfactant can still act as a template and whether STS can still be formed.

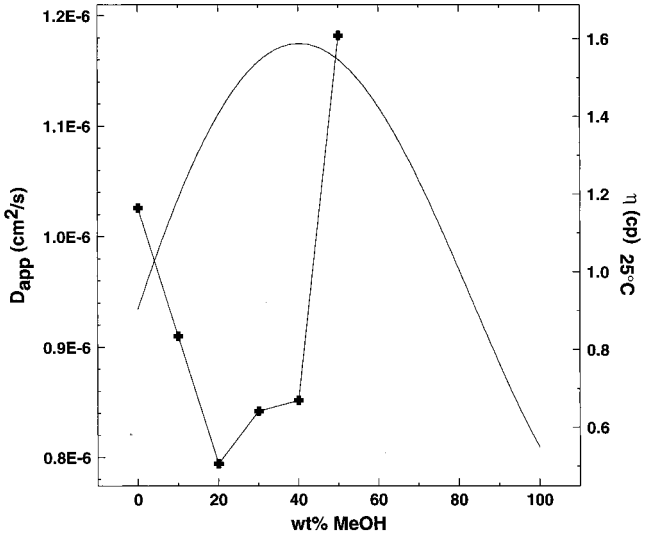

Figure 5. Apparent diffusion coefficient of micelles (in a water/methanol/CTAB/NaOH solution with molar ratios as in Table 1) (plusses) and solvent viscosity (solid curve) plotted against methanol concentration. From these data the hydrodynamic radius of the micelles can be determined.

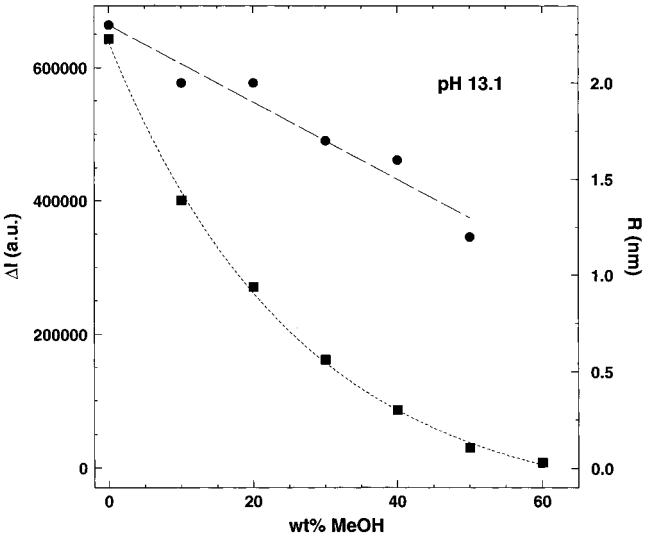

Figure 6. The hydrodynamic radius of the micelles (circles) in a water, methanol, CTAB, NaOH solution (molar ratios as in Table 1) is found to decrease with increasing methanol concentration, and the scattering intensity (squares) decreases much more rapidly, which indicates that at $r = 60\%$, micelles essentially cease to form.

3.3. Base Concentration. *3.3.1. Effects of NaOH on Micelle Formation.* Figure 7 shows the 8-fold increase of the micelle scattering intensity with increasing NaOH concentration, an increase not associated with a significant change in the cmc. The increase in scattering intensity could be a pH effect or may be due to the

(34) Czerniawski, M. *Roczn. Chem.* **1966**, *40*, 1935.

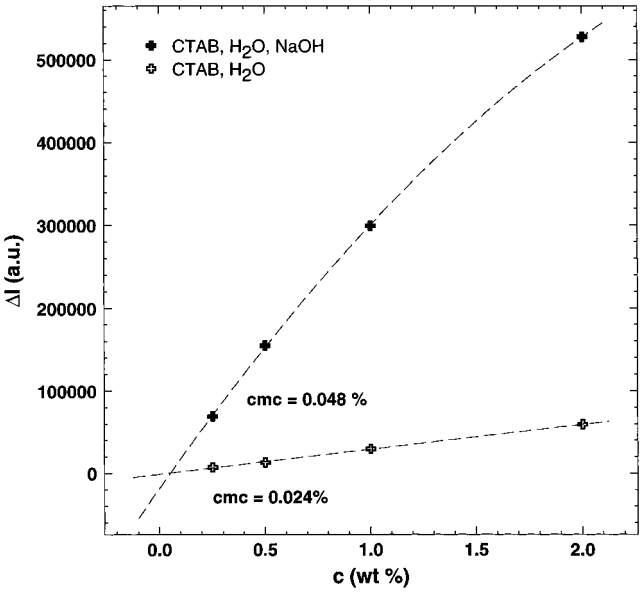

Figure 7. Sodium hydroxide is found to greatly increase the scattering intensity of a CTAB solution, and yet does not significantly alter the cmc. Note that *c* is the concentration of CTAB and the molar ratios are water/CTAB/(NaOH) = 129.6: 0.130:(0.289).

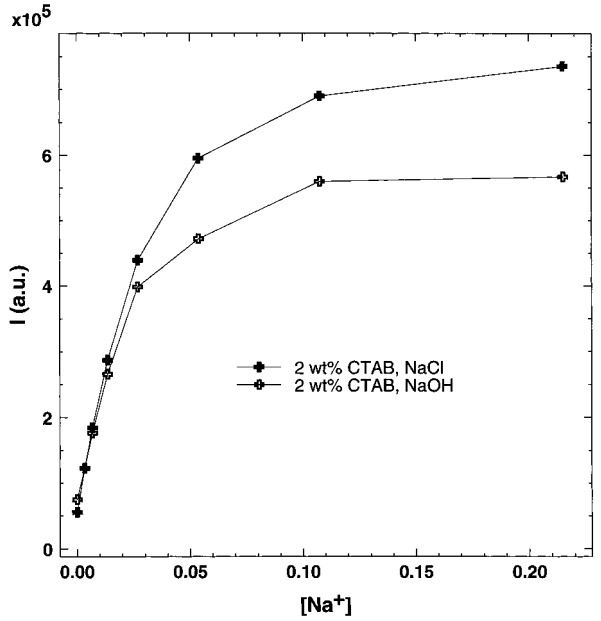

Figure 8. The increase in the scattering intensity we observe with NaOH can be achieved by adding NaCl, indicating that the effect is not one of pH but is due to the increased ionic strength of the solution.

increased ionic strength of the basic solution. Figure 8 shows that adding NaCl to the solution causes an increase in scattering intensity similar to that found with NaOH, so we believe that an increase in the micelle size may occur due to charge screening: The additional counterions aid in screening the charge interaction between the cationic headgroups, reducing the electrostatic contribution to the micelle energy and allowing larger micelles to form.

Such ionic screening effects have been observed in similar systems.[31,32,35] To determine the effect of salt directly, we used DLS to determine the dependence of the diffusion coefficient and hydrodynamic radius on

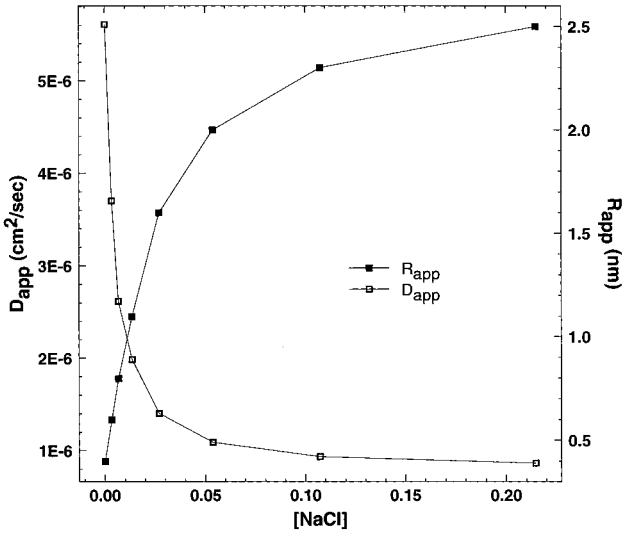

Figure 9. Dynamic light scattering measurements on 2 wt % CTAB at neutral pH. With added salt, the diffusion coefficient decreases and the hydrodynamic radius increases. The larger micelle size indicates the formation of full micelles at high salt concentration, which causes the increased scattering of light.

salt concentration (Figure 9). These data show that the hydrodynamic radius increases from 0.4 nm at [salt] = 0 to 2.5 nm at [salt] = 0.215 M. The radius of a spherical micelle should be about 2.0 nm, so the very small aggregates we observe may only be poorly organized clusters of several molecules. In any case, the micelle size and mass are dependent upon the ionic strength of the solution.

3.3.2. Effect of NaOH on STS Formation. Figure 10 shows how X-ray diffraction was used to optimize the NaOH concentration. The figure shows that the relative intensity of the 100 Bragg peak is a maximum at a Si/NaOH ratio of about 0.29. This ratio (0.289) was thus used in all of the subsequent preparations reported here, as shown in Table 1. At Si/NaOH ratios greater than ~1.0 a clear homogeneous solution persists after all of the reagents are mixed. For Si/NaOH ratios greater than 1.4 and less than 2.2, large hexagonally faceted crystals form in solution after about 1 day. X-ray diffraction confirms that the crystals have a lamellar structure and that the basal spacing is approximately 30 Å (00*l* reflections with $l = 1-9$ are observed). Attempts to isolate the crystals and examine them with single-crystal X-ray diffraction were not successful, as the crystals warped and fractured when dried in air.

Interestingly, addition of 1 N HCl at times less than 1 day to the clear, homogeneous solutions that have Si/NaOH > 1.0 leads to the formation of hexagonal periodic mesoporous silica. In the "back-titration", enough HCl is added to the solution to lower the Si/NaOH ratio to approximately 0.3. Ordered STS that exhibits four Bragg peaks has been made with this approach.

3.4. Effect of Methanol Concentration on Micellization and STS Order. The coherent scattering domain size, CSD, is a measure of the long-range order

(35) Nicoli, D. F.; Ciccolello, R.; Briggs, J.; Dawson, D. R.; Offen, H. W.; Romstead, L.; Bunton, C. A. In *Scattering Techniques Applied to Supramolecular and Nonequilibrium Systems*; Chen, S., Chu, B., Nossal, R., Eds.; NATO Advanced Study Institute Series, Series B: Physics; Plenum: New York, 1981; Vol. 73, p 363.

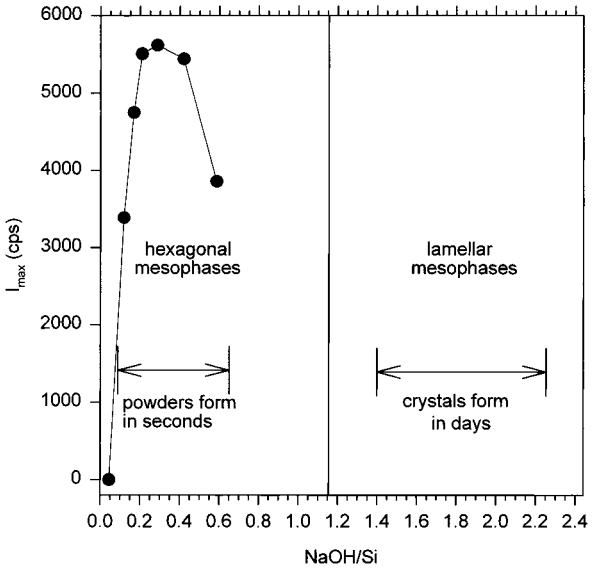

Figure 10. X-ray diffraction intensity of the 100 Bragg reflection plotted against NaOH concentration. The data were collected on $r = 25\%$ samples with equal scattering volumes under nominally identical instrumental conditions with molar values as in Table 1 (except for NaOH). For NaOH/Si < 1.0, periodic mesophase gels form in seconds (if pH > 8). For NaOH/Si > 1.4, transparent crystals that have a lamellar structure grow in solution in a few days.

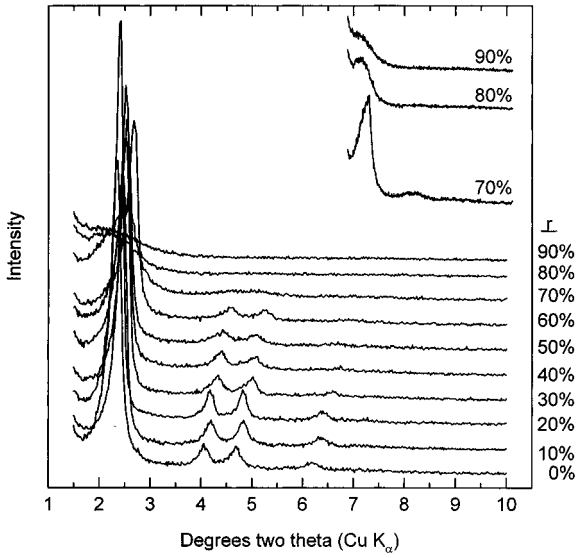

Figure 11. X-ray diffraction data for samples prepared from molar ratios shown in Table 1 and aged for 1 day at room temperature (to prepare the samples, TMOS was added to the precursor solutions used to obtain data in Figure 6). The number of Bragg reflections decreases as r increases, which indicates a reduction in long-range order of the hexagonally packed pores. The $r = 70-90\%$ samples were washed with methanol only to avoid the possibility of conversion of unreacted reagents to STS. Adding water to the filtrate produced no solids.

of the hexagonally packed pores in STS. It is determined by applying the Scherrer equation to the diffraction data (Figure 11):

$$\mathrm{CSD} = \Delta(2\theta)_{\mathrm{sample}} - \Delta(2\theta)_{\mathrm{inst}} = 0.9\lambda/L \cos \theta_{\mathrm{sample}} \quad (2)$$

where $\Delta(2\theta)_{\mathrm{sample}}$ is the fwhm of the Bragg diffraction peak in radians, $\Delta(2\theta)_{\mathrm{inst}}$ is the instrumental broadening of the peak in radians,[37] λ is the incident radiation

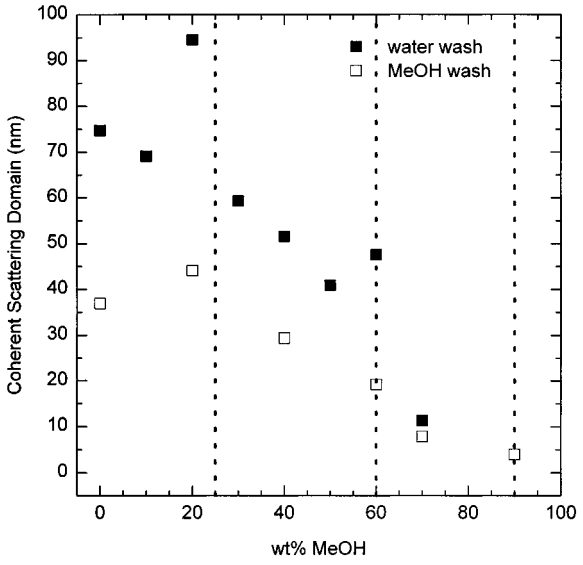

Figure 12. Coherent scattering domain CSD size determined by analysis of the diffraction data in Figure 11 and others (MeOH wash). The long-range order of the mesophases is found to be a maximum at $r = 20-25\%$ for samples washed with water (circles) and for samples washed with methanol (triangles). There is a precipitous drop in CSD at $r = 60\%$; $c - \mathrm{cmc} = 0$.

wavelength (1.54056 Å), θ_{sample} is the peak position, and L is the coherent scattering domain (CSD) size in angstroms. In all cases, the observed particle size of the products (150+ nm) is larger than the CSD size, so the broadening of the Bragg peaks is a measure of the long-range order within a particle, rather than a measure of particle size.

Figure 12 shows the evolution of CSD with methanol concentration. The CSD generally decreases with methanol concentration, but there is a sharp maximum at 20−25% for both water- and methanol-washed samples. The general decrease in CSD with methanol concentration including the abrupt decrease at high methanol concentration (excepting the maximum at 20−25%) parallels that observed for the degree of micellization with methanol concentration; compare Figures 12 and 4. The increase in CSD for $r = 20-25\%$ is real and has been confirmed on more than five samples; $r = 25\%$ is also the minimum value for which STS forms out of homogeneous solutions (t_{diss} exceeds t_{gel}). Therefore, we suspect that solution homogeneity affects CSD, and we observe that the samples with the largest CSD*s* are formed from homogeneous solutions, even though the micelle concentration is less than in pure water.

The STS samples made with $r \geq 70\%$ are of particular interest, as the precursor solution contains no micelles prior to TMOS addition. The X-ray diffraction patterns exhibit one broad Bragg peak at $d = \sim 41$ Å in the XRD pattern, characteristic of disordered STS (resembles wormlike structures observed by others).[22,38]

There is a large but finite range for which disordered STS forms ($70\% \leq r \leq 90\%$). At $r > 90\%$ the silicate

(36) Firouzi, A.; Kumar, D.; Bull, L. M.; Besier, T.; Sieger, P.; Huo, Q.; Walker, S. A.; Zasadzinski, J. A.; Glinka, C.; Nicol, J.; Margolese, D.; Stucky, G. D.; Chmelka, B. F. *Science* **1995**, *267*, 1138.

(37) The instrumental peak breadth (fwhm), as determined by using an Ag-boehmite standard in conjunction with data from a NIST Si standard, is $\Delta(2\theta)_{\mathrm{inst}} \approx 0.10°$ for the *100* Bragg reflection.

(38) Ryoo, R.; Kim, J. M.; Co, C. H.; Shin, C. H. *J. Phys. Chem.* **1996**, *100*, 17718−17721.

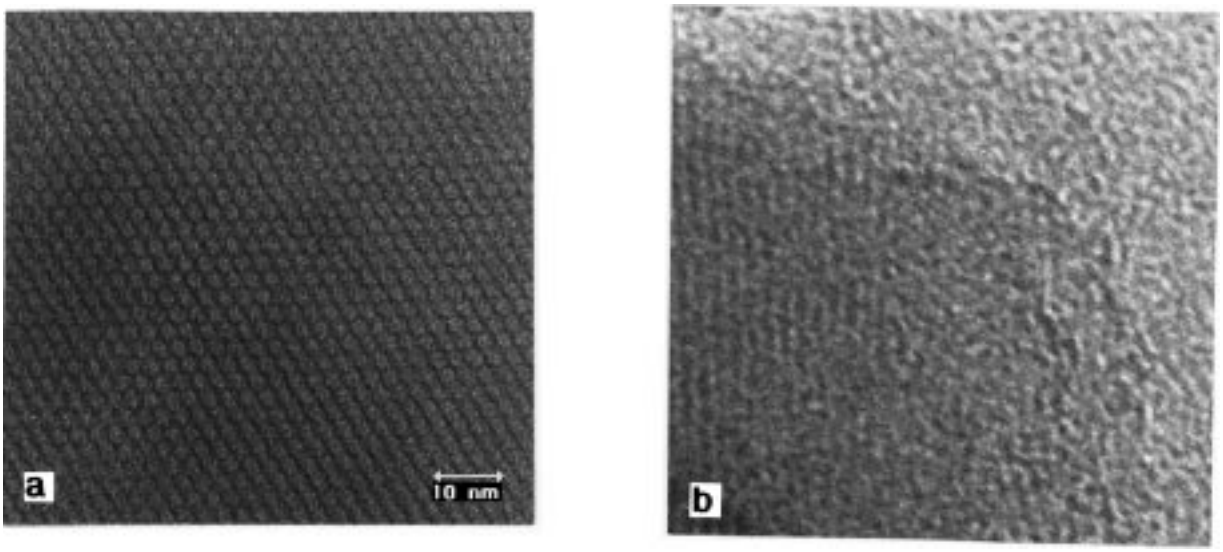

Figure 13. Transmission electron micrographs (identical scale) of uncalcined samples aged for 1 day at room temperature (exact samples used to determine CSD and cell constants in Table 1). (a) $r = 30\%$ sample showing regular honeycomb arrangement of pores over a very large area, consistent with four sharp Bragg peaks in the XRD pattern and a relatively large CSD. The pore size is estimated to be 33 ± 3 Å. (b) $r = 70\%$ showing a disordered arrangement of pores, consistent with one broad Bragg peak in the XRD pattern and a small CSD.

Table 2. Data on Porous Mesophases[a]

r (%)	aging times[b]	a_{powder} (Å)[c]	a_{calcd} (Å)[d]	shrinkage (%)	calcd gas(es)	hold time(s) at 550 °C (h)	heating rate (°C/min)	SA (m^2/g)[e]	V_p (cc/g)[f]	P/P_o uptake[g]
0	50 h/17 days	43.3 (3)	38.7 (3)	10.6	N_2/O_2	4/20	10	844 (8)	0.60	0.17−0.27
25	50 h/17 days	39.7 (5)	35.6 (3)	10.3	N_2/O_2	4/20	10	650 (9)	0.36	0.10−0.18
25	72 h/42 days	41.6 (5)	35.9 (6)	13.7	O_2	10	1	973 (10)	0.54	0.11−0.19
25[h]	40 h/150 days	45.4 (1)	38.4 (1)	15.3	O_2	2	4.4	902 (10)	0.56	0.16−0.23
25[i]	40 h/150 days	45.3 (1)	37.3 (1)	17.7	O_2	2	4.4	651 (11)	0.42	0.12−0.23
70	50 h/17 days	∼43	<34[j]	>21	N_2/O_2	4/20	10	317 (5)	0.18	0.10−0.18

[a] Molar ratios as in Table 1. [b] Aging times of wet gel in pore fluid/dried gel at ambient conditions before calcination. [c] Cell constant of dried powder. [d] Cell constant of calcined powder. [e] Surface area (4-point BET from N_2 sorption). [f] Single point total pore volume at $P/P_o > 0.90$. [g] Range of P/P_o for which a steep uptake of nitrogen, with a positive deviation in slope from lower P/P_o values, is observed. [h] Made with C_{16}TMACl. [i] Made with C_{16}TMA $C_7H_7SO_3$ (cetyltrimethylammonium *p*-toluenesulfonate). [j] Only one broad, weak peak in XRD; cell constant quite uncertain.

polyanions and surfactant molecules are no longer able to organize into superstructures, and translucent amorphous chemical gels form. Gelation times here are typically at least 2 orders of magnitude longer than for mesophases (i.e., several hours). The water/silicon ratio is less than 10 in this regime. In this methanol-rich solvent, it is clear that the surfactant has ceased to act as an effective chemical dipole, probably owing to the lower dielectric constant and weaker hydrogen bonding of methanol, and that the impetus for cooperative assembly into an ordered product is gone.

To summarize, the materials that have the largest CSD sizes[39] are made from solutions that are homogeneous at the gel point and for which cmc is high; for the conditions studied here (Table 1), $r = \sim 20-25\%$. The STS structure transforms from ordered hexagonal (3 Bragg peaks) to disordered (1 Bragg peak) at $r > 60\%$. The extent of micellization and the order/structure of STS evolve similarly with methanol concentration; i.e., both decrease until $r \approx 60\%$ and then show a discernible change (above cmc to below cmc and order to disorder).

(39) The surfactants are nominally 99+% pure. The primary impurities are assumed to be aliphatic and hydrophobic, and they most likely reside inside at the hydrophobic interior of the micelle. Such species are more soluble in alcohol than in water. Partitioning of these species into the continuous phase could increase the dispersity of micelles. This could lead to an increase in CSD size and may contribute to the increase in CSD size.

3.5. Structures of Ordered and Disordered STS. The effect of methanol concentration on the real space long-range order is illustrated in Figure 13 which shows transmission electron micrographs of samples made from homogeneous solutions above (a) and below (b) cmc. Figure 13a illustrates the long-range order of hexagonally packed pores that can be achieved by synthesizing samples from homogeneous solutions with near maximum values of $c -$ cmc. Figure 13b shows that much of the sample has no discernible order and appear wormlike.[22,36] The parallel lines on the left of the micrograph are uncommon, and are believed to be representative of the maximum order in these samples. The TEM data thus corroborates the XRD data, showing a progressive decrease in the order of the pore system as r increases from 30% to 70%. From the XRD data, which show one broad Bragg peak, we believe that the samples made with $r = 80\%$ and 90% have a structure very similar to that seen for $r = 70\%$.

3.6. Sorption Studies. Figure 14 shows the nitrogen sorption isotherms for identically prepared and calcined $r = 0\%$, 25%, and 70% STS (see Table 2, entries 1, 2, and 6, for experimental details). The periodic porosity in the $r = 0\%$ sample is indicated by the steep increase in nitrogen uptake between relative pressures of 0.17 and 0.27. As is discussed in the paper by Ravikovitch et al.,[40] this type of isotherm is expected

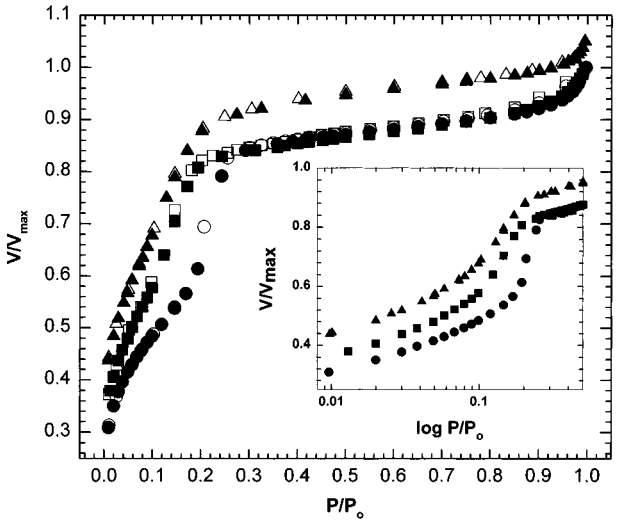

Figure 14. Nitrogen sorption isotherms plotted on reduced axes for data collected at 77 K on identically prepared and calcined $r = 0\%$ (circles), 25% (squares), and 70% (triangles) samples. The filled symbols show adsorption; the closed symbols, desorption. For clarity 0.05 has been added to the actual V/V_{max} value for the $r = 70\%$ sample. The inset shows the low P/P_o region plotted on a log axis, with no distinction between adsorption and desorption points. The molar ratios used to prepare the samples are in Table 1; calcination and porosity data are in Table 2.

for STS materials with pores less than about 40 Å in diameter, and the steep uptake is consistent with pore filling. The $r = 25\%$ and 70% samples also show an increased uptake of nitrogen in the 0.10−0.18 P/P_o region, although it is less pronounced than for the $r = 0\%$ sample.

The three isotherms resemble Type IV isotherms, but clearly are not classical. As the steep increase in nitrogen uptake occurs at $P/P_o < 0.42$, it is not appropriate to use the Kelvin equation to analyze the sorption data. Lacking an adequate theory to determine pore diameters and distributions for these isotherms, we suffice it to say that the pore diameter decreases as r increases, as indicated by the shift in the steep uptake of nitrogen to lower relative pressures.

3.7. Template, Cell, and Pore Sizes. The data show that as the methanol concentration increases, the template size, cell size, and pore size decrease. Figure 15 shows that as r is increased from 0% to 60% (molar ratios given in Table 1), the unit cell constant of STS decreases monotonically. The slight increase in cell size for $r = 70\%$ may be indicative of a slightly different formation mechanism associated with assembly from a nonmicellar system, or simply with the change from an ordered structure to a disordered structure. Figure 6 shows that as r is increased from 0% to 60%, the micelle radius also decreases monotonically. A decrease in micelle diameter of the E hexagonal liquid crystalline phase from 45 Å (water) to 38 Å (ethanol) has been observed in simple CTAB/water versus CTAB/ethanol systems.[26] The measured decrease in micelle diameter in the CTAB/water/methanol system is consistent with this previous work. Figure 14 implies that the pore diameters also decrease. Note that the steep uptakes

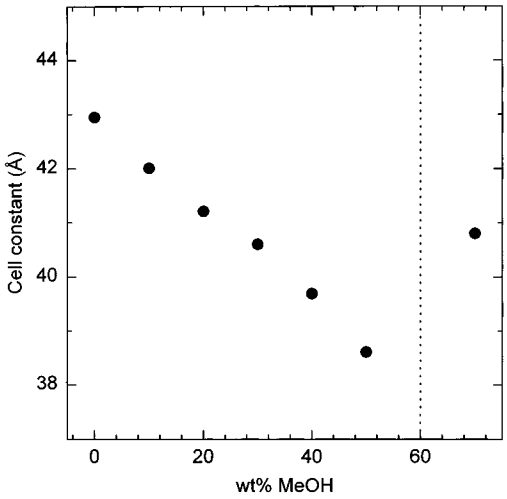

Figure 15. Unit cell parameters (Table 1) and pore radii decrease (Table 2) as r increases until $r = 60\%$ (c − cmc = 0), which parallels the decrease seen in the micellar radius with increasing r (Figure 6). At $r = 70\%$ (c − cmc < 0), the pore diameter and the unit cell parameter increase, perhaps indicating a different assembly mechanism when no micellar templates are initially present.

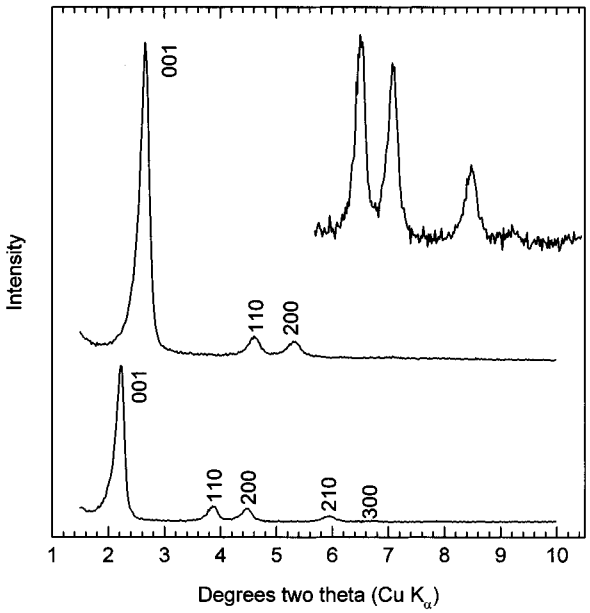

Figure 16. X-ray diffraction of a calcined $r = 25\%$ sample (Table 2, CTACl) showing that the long-range order of the calcined product is less than for that of the uncalcined, as evidenced by the absence of the 210 and 300 Bragg reflections. Note the shift of the peaks to high 2θ values in the calcined sample, which indicates a shrinkage of the unit cell.

in the $r = 25\%$ and 70% samples are nearly identical, as are their cell constants, which implies that their wall thicknesses are quite similar. Thus, the general conclusion is that changing r provides continuous control over the template size, which allows control of the cell constant of STS over a ∼5-Å interval, and allows the pore diameter to be decreased.[41]

Table 2 gives data for several $r = 25\%$ samples that give an indication of the variability of cell constants,

(40) Ravikovitch, P. I.; Ó Domhnaill, S. C.; Neimark, A. V.; Schüth, F.; Unger, K. K. *Langmuir* **1995**, *11*, 4765−4772.

(41) Stepwise control of pore diameter has also been demonstrated in the $r = 25\%$ series by using $C_nH_{2n+1}N(CH_3)_3Br$ with $n = 10$, 12, 14, 16, or 18. The cell constant changes approximately $\Delta n \times 2.25$ Å in this range, which is very similar to what has been found in purely aqueous systems.[1,3]

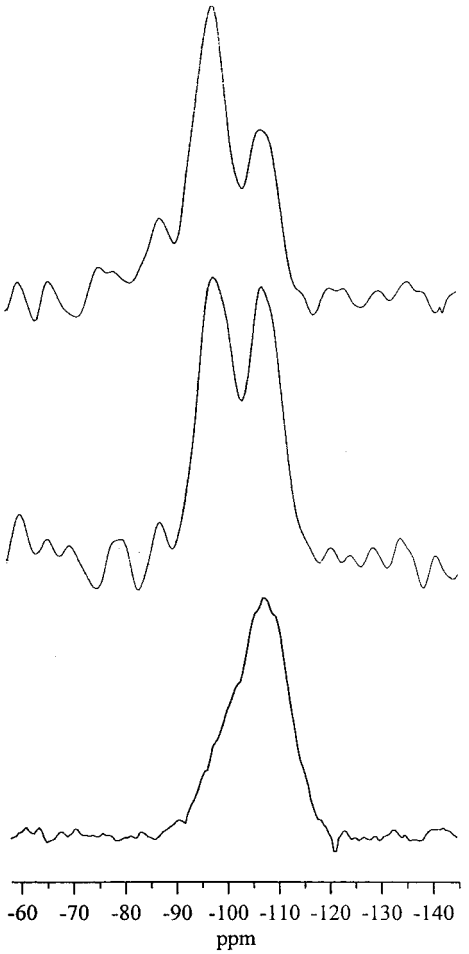

Figure 17. ^{29}Si MAS NMR on $r = 25\%$ samples shows that after 10 min (top) the samples are very poorly condensed ($Q^3/Q^4 = 2.1$) but that when aged at room temperature for 7 days in their mother liquor (middle), they continue to condense ($Q^3/Q^4 = 1.2$), until, finally, after calcination, they form a strong siloxane framework (bottom, $Q^3/Q^4 \approx 0.40$). Peak positions: 1 min − $Q^2 = -88.2$ ppm, $Q^3 = -98.8$ ppm, $Q^4 = -107.8$ ppm; 7 d − $Q^2 = -87.6$ ppm, $Q^3 = -98.5$ ppm, $Q^4 = -107.8$ ppm; calcined − $Q^2 = -88.8$ ppm, $Q^3 = -98.0$ ppm, $Q^4 = -106.7$ ppm.

shrinkage, surface area, pore volume, nitrogen uptake depending upon aging time, calcination schedules, and surfactant counterion type. Note that surface areas as large as 973 m^2/g and pore volumes up to 0.56 cm^3/g have been achieved. In all cases, the long-range order decreases in the calcined versus as-made materials, as evidenced by the presence of fewer and broader diffraction peaks (Figure 16).

3.8. Framework Condensation. Figure 17 shows ^{29}Si MAS NMR spectra for $r = 25\%$ powders isolated 1 min after formation, aged 7 days, and calcined. As expected, there is a very high fraction of uncondensed silica species present in the product isolated after 1 min. The Q^3/Q^4 ratio is ∼2.1 as compared to ∼1.1 for a material made from TEOS in water (isolated after 10 min; this work). Figure 18 shows that $r = 25\%$ samples aged only 5 min can be calcined immediately without collapse to yield a porous product.

Samples can also be aged at room temperature in their mother liquor for long periods of time to promote ambient temperature siloxane bond formation. For a sample aged 1 week, the Q^3/Q^4 ratio nearly halves to ∼1.2, which is comparable to the TEOS-dervied sample isolated shortly after formation.

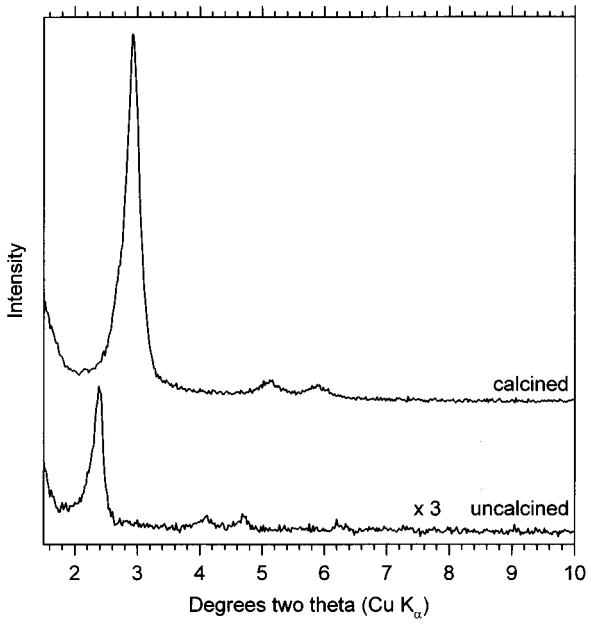

Figure 18. X-ray diffraction on the uncalcined $r = 25\%$ sample aged 10 min shows four diffraction peaks, indicative of PMS. 0.49 g of the wet, suction-filtered gel was immediately placed into a calcination dish, put into a tube furnace with flowing O_2, ramped at 10 °C/min to 550 °C, held for 10 h, and then cooled to room temperature with the furnace off. 0.055 g of calcined material was recovered. X-ray diffraction on the calcined materials shows three diffraction peaks, indicative of PMS, which shows that the silica framework does not collapse in calcination even after very short aging times.

After the aged, TMOS-derived sample is calcined, the Q^3/Q^4 ratio is ∼0.40, which is nearly identical to that for samples made from TEOS (0.3−0.5)[4] and similar to those reported for calcined hydrothermal samples (∼0.25). The similarity is important, as it means that the framework from the kinetic TMOS-derived samples is ultimately as well condensed as materials made from other alkoxysilanes.

3.9. Microstructure. The tertiary structure of the TMOS-derived periodic products is distinctly different from materials made from nonmolecular sources[1,2,6] or from $Si(OR)_4$ where R = C_2H_5, C_3H_7, or C_4H_9 (this work). TMOS gives weak particulate gels rather than colloidal precipitates. The morphology of the product differs substantially depending on whether methanol is used as a cosolvent or not. Figure 19 shows that for $r = 0\%$ the material is dimorphic, consisting of micron-long faceted tubules and submicron aggregated ellipsoids; for $r = 25\%$ the material exhibits a uniform microstructure of submicron aggregated spherical and ellipsoidal particles. SEM on an $r = 70\%$ sample shows only circular particles (presumably spherical) that range from 0.15 to 1.5 μm in diameter. The microstructure of the powders provides ready access to the internal surfaces of each submicron crystallite. We have examined the structure and absorptive properties of the gel *monoliths*, and details are reported elsewhere.[23,24]

4. Conclusions

The methanol concentration affects the degree of micellization in the presilicate surfactant solution as

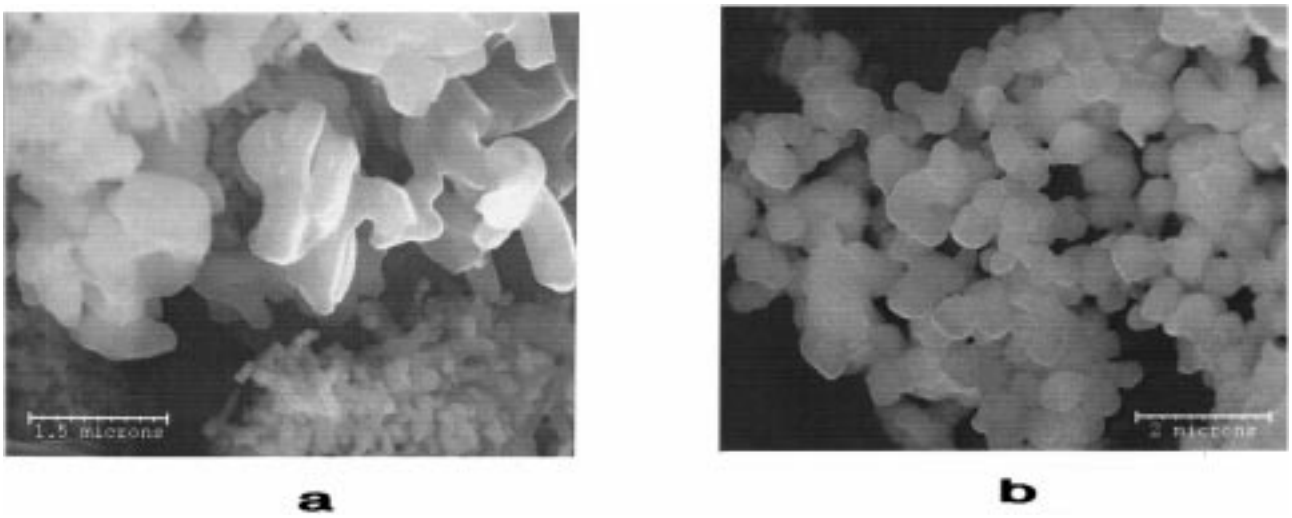

Figure 19. Scanning electron microscopy on (a) an $r = 0\%$ sample showing two distinctly different primary particle sizes and morphologies and (b) an $r = 25\%$ sample showing a uniform microstructure, consisting of aggregated spherical and ellipsoidal submicron crystallites. The larger crystallites in panel a show sharp edges and grow as tubules, whereas the smaller crystallites are smoother and spherical or ellipsoidal.

well as the coherent scattering domain size/structure of STS. Additionally, the use of methanol allows the template size and concentration, cell constant, and pore diameter to be continuously tuned. Methanol also permits the rapid dissolution of TMOS in the solvent system, allows STS to be formed from homogeneous solutions, lowers the Kraft point of CTAB below 25 °C, and virtually eliminates foaming during suction filtration. The optimal long-range order of STS occurs for a water/methanol ratio of ~75:25. The use of TMOS as the silica source increases the formation kinetics and leads to the formation of particulate gels rather than colloidal precipitates. The morphology and minimal connectivity of particles in the STS gels may be advantageous for gas adsorption applications. The inorganic framework of the STS gels is initially poorly condensed, but aging and calcination provide a well condensed, stable siloxane network.

Acknowledgment. We thank Celeste Drewien for the high-resolution electron microscopy and R. Assink (SNL) and S. Prabakar (UNM) for the NMR data. We thank the reviewers for many helpful comments and suggestions. This work was funded by the United States Department of Energy under Contract No. DE-AC04-94AL85000. Sandia is a multiprogram laboratory operated by Sandia Corporation, a Lockheed Martin Company, for the United States Department of Energy.

CM970240M